Mon. Not. R. Astron. Soc. **000**, 1–5 (2013) Printed 8 November 2013 (MN LATEX style file v2.2)

Modelling the X-ray emission of the O3+O6 binary HD 150136 via a wind-star collision

C. M. P. Russell[1⋆], A. T. Okazaki[1], S. P. Owocki[2], J.-C. Leyder[3], A. M. T. Pollock[3], and M. F. Corcoran[4,5]

[1] *Faculty of Engineering, Hokkai-Gakuen University, Toyohira-ku, Sapporo 02-8605, Japan*
[2] *Department of Physics & Astronomy, University of Delaware, Newark, DE 19716, USA*
[3] *European Space Agency, European Space Astronomy Centre, P.O. Box 78, E-28691 Villanueva de la Cañada, Spain*
[4] *NASA/GSFC, Greenbelt, MD 20771, USA*
[5] *Universities Space Research Association, Columbia, MD 21044, USA*

Accepted 2013 XXXX XX. Received 2013 XXXX XX; in original form 2013 November 07

ABSTRACT

HD 150136 is a short-period (2.675 d), O3+O6 binary system harbouring the nearest O3 star. The literature wind parameters suggest that the stronger O3 primary wind will overwhelm the O6 secondary wind along the line between the stars and induce a 'wind-star collision' (WSC). We use 3D smoothed particle hydrodynamics (SPH) to model this WSC, as well as the wind-wind collision (WWC) produced off-axis, to discern the density and temperature structure of the shocked winds, and then perform 3D radiative transfer to compute the X-ray properties of the system. The model qualitatively reproduces the *Chandra* X-ray light curve obtained around superior conjunction, and could reproduce this observation in absolute flux depending on the contribution of embedded-wind-shock X-rays. The model spectra match well in the soft band and show the same strong lines as the data, although the hard flux is underestimated. The full-orbit model light curve predicts an asymmetry in the unobserved portion of the orbit due to the difference in the leading vs. trailing sides of the WSC and WWC shocks, which we will test in a follow-up paper.

Key words: stars – binaries: HD150136, SPH, radiative transfer, X-rays

1 INTRODUCTION

HD 150136, located in NGC 6193 near the center of the Ara OB1 association, is an important system since it harbours the nearest O3 star (Herbst & Havlen 1977). The close companion, which is an O6 star in a circular, 2.675-day orbit (Mahy et al. 2012, hereafter M12), provides a unique probe of the primary star at a multitude of wavelengths. In this letter, we focus on interpreting the *Chandra* X-ray observations carried out by Skinner et al. (2005, hereafter S05), which covered a third of the orbital phase. The light curve varied significantly, dropping by ∼30% and then recovering to its initial value. This behavior was originally attributed to the more distant third star (O7, ∼8–15 yr period) passing between the observer and the central binary since the observation was thought to be taken at quadrature. The refinement of the orbital ephemeris by M12, however, showed that the *Chandra* observation was actually taken around superior conjunction, leading to the natural explanation that increased absorption from the O3 wind caused the observed decrease in X-ray flux.

This work aims to reproduce the *Chandra* observation of HD 150136 from 3D hydrodynamic simulations of its colliding stellar winds, and 3D radiative transfer to synthesize the X-ray properties. The modeling is sensitive to the stellar, wind, and orbital parameters, so it can provide constraints on these parameters, and/or confirm the literature values.

Section 2 discusses the hydrodynamic modeling and radiative transfer. Section 3 compares the results of the X-ray radiative transfer with the *Chandra* observation, and details the model predictions for the remainder of the orbit. Sections 4 & 5 discuss the results and conclude the work.

2 MODEL DETAILS

2.1 3D Hydrodynamics

We apply the 3D SPH code developed through Benz et al. (1990), Bate et al. (1995), Okazaki et al. (2008), Russell (2013, hereafter R13), and Madura et al. (2013) to model

⋆ E-mail: crussell@udel.edu; Animations available upon request.

© 2013 RAS

Table 1. Stellar, wind, and orbital parameters of HD 150136 (M12, using their best inclination) used in the SPH simulations.

Parameter	O3 (Primary)	O6 (Secondary)
M ($M_\odot$)	64	41
R ($R_\odot$)	13	9.5
L ($L_\odot$)	7.24×10^5	1.06×10^5
$T_{\rm eff}$ (K)	4.65×10^4	
$\dot{M}$ ($M_\odot$/yr)	1.0×10^{-6}	7.0×10^{-8}
v_∞ (km/s)	3500	2500
P (days)	2.675	
e	0.0	
a (cm) [AU]	2.66×10^{12} [0.178]	
i (°)	49	

the central colliding-wind binary (CWB) of HD 150136. The stars $i=1,2$ are represented by point masses of radius R_i that inject SPH particles in a random distribution from a sphere $r_{{\rm inj},i}$ just outside R_i. The anti-gravity-like radiative forces that drive these stellar wind particles are tuned such that, when a particle only experiences radiation from its star, the winds follow a $\beta=1$ velocity law, i.e. $v_i(r_i) = v_{\infty,i}(1-R_i/r_i)$, where $v_{\infty,i}$ is wind i's terminal velocity. Each wind experiences accelerations from both radiation fields, so the velocity-altering component of radiative inhibition (Stevens & Pollock 1994) is included in this formalism. The particles are injected with temperature $T_{\rm eff}$ at the position where $v(r_{{\rm inj},i}) = 2c_s$, where c_s is the sound speed. This alleviates the difficult task of accelerating the wind through the sonic point, which has not yet been achieved in 3D hydrodynamic simulations of CWBs, but requires the mass flux to be chosen *a priori*, so the mass-loss-rate-altering component of radiative inhibition is not included. The SPH code implements optically-thin radiative cooling using the Exact Integration Scheme (Townsend 2009) with a cooling function $\Lambda(T)$ from `CLOUDY` 90.01 (Smith et al. 2008) for solar abundances. To account for the stellar heating of the unshocked wind material, which keeps the gas at approximately $T_{\rm eff}$ (Drew 1989), the floor temperature of the simulation is set to $T_{\rm floor}=T_{\rm eff}$. Further information about the SPH code can be found in R13 and Madura et al. (2013).

Table 1 gives the stellar[1], wind, and orbital parameters for HD 150136 (M12). Typical CWBs have their wind-wind collision (WWC) region located between the stars where the ram pressures of their winds are equal, but for this system, the O3-wind ram pressure is greater its counterpart throughout the region between the stars (for the assumed $\beta=1$ law); this leads to the O3 wind colliding directly with the surface of the O6 star. The potential wind-star collision (WSC) can be altered by the phenomenon of radiative braking (Gayley et al. 1997), where the O3 wind would be decelerated and eventually stopped by the O6 radiation before reaching the O6 surface. However, the current literature values suggest the O6 radiation ($L_2=2.1\times10^5 L_\odot$, M12) is not strong enough to radiatively brake the incoming wind (R13).

[1] The L_2 value used in the SPH simulations is calculated by requiring the parameters to obey the Castor et al. (1975) scaling $L_2/L_1 = (M_2/M_1)^{1-\alpha}\left(\dot{M}_2/\dot{M}_1\right)^{\alpha}$ where the ensemble line strength parameter is taken to be a typical value of $\alpha=2/3$.

Since the O3 wind is much stronger than the O6 wind, and radiative braking should not occur, the SPH code for HD 150136 needs to model the WSC. Wind particles that reach the stellar radius R_i are absorbed by the point masses, but the final accretion onto the star should be at approximately the sound speed (Owocki et al. 1994). To do this, we introduce 'ghost SPH particles' as a means to decrease the O3-wind velocity along the radial direction of the O6 star. For O3 SPH particles that come within two smoothing lengths (which is the extent of the sphere of influence of an SPH particle in the standard SPH kernel (Monaghan 1992) adopted in this work) of R_2, a ghost particle of the same particle mass, opposite radial velocity, and equal tangential velocity is created in a position radially opposite R_2, i.e. $r_{\rm ghost} = 2R_2 - r_{\rm particle}$. The end result is a stronger shock near the O6 surface that has approximately twice as many O3 particles (equivalent to about double the volume of O3 gas) at X-ray emitting temperatures than in simulations without ghost particles, thus producing more X-ray emission from the WSC.

Fig. 1 shows a single output of density (left) and temperature (right) in the orbital plane. As expected, the O3 wind reaches the surface of the O6 star, and the off-center material forms a WWC shock cone with a half-opening angle of $\sim40°$, which is skewed by orbital motion. Both the WSC and WWC regions are hot, but the WSC is hotter due to its head-on collisions versus the oblique WWC collisions. Thus the majority of X-ray emission should come from the WSC.

2.2 3D X-ray Radiative Transfer

To compute the X-ray emission from colliding winds in HD 150136, we perform 3D radiative transfer on the density and temperature structure of the SPH simulations. This involves solving the formal solution to the equation for radiative transfer for a grid of 1D rays throughout the simulation volume, for which the SPH visualization program `Splash` (Price 2007) is our basis. The emissivity $j(E)$ at energy E is $j(E) = n_e n_H \Lambda(E,T)$, where n_e and n_H are the electron and hydrogen number densities, and $\Lambda(E,T)$ is the emission function generated from the `APEC` model (Smith et al. 2001) in `XSpec` (Arnaud 1996), computed for a logarithmically spaced grid of 78 temperatures T from 10^5–7×10^8 K and 170 energies from 0.2–10 keV. For circumstellar absorption by the winds, the opacity κ_E is from a `windtabs` model (Leutenegger et al. 2010) with O-star abundances (specifically for 30,000 K, although value does not significantly affect the radiative transfer calculation over the *Chandra* band pass). For the interstellar medium absorption of $N_H = 4\times10^{-21}\,{\rm cm}^{-2}$ (S05), $\kappa_E^{\rm ISM}$ is computed from the `tbabs` model (Wilms et al. 2000) in `XSpec`. The end result of the radiative transfer is one pixel map per energy that are then summed to determine the spectra. Assuming a distance of 1.32 kpc (Herbst & Havlen 1977), the model spectra are folded through the *Chandra* response function to directly compare with the observations of HD 150136. Since the orbit is circular, the phase dependence of the radiative transfer is calculated by moving the observer perspective around the stars, using density and temperature outputs that are significantly after the simulation volume has been filled.

Fig. 2 shows the 1 keV surface brightness maps of the

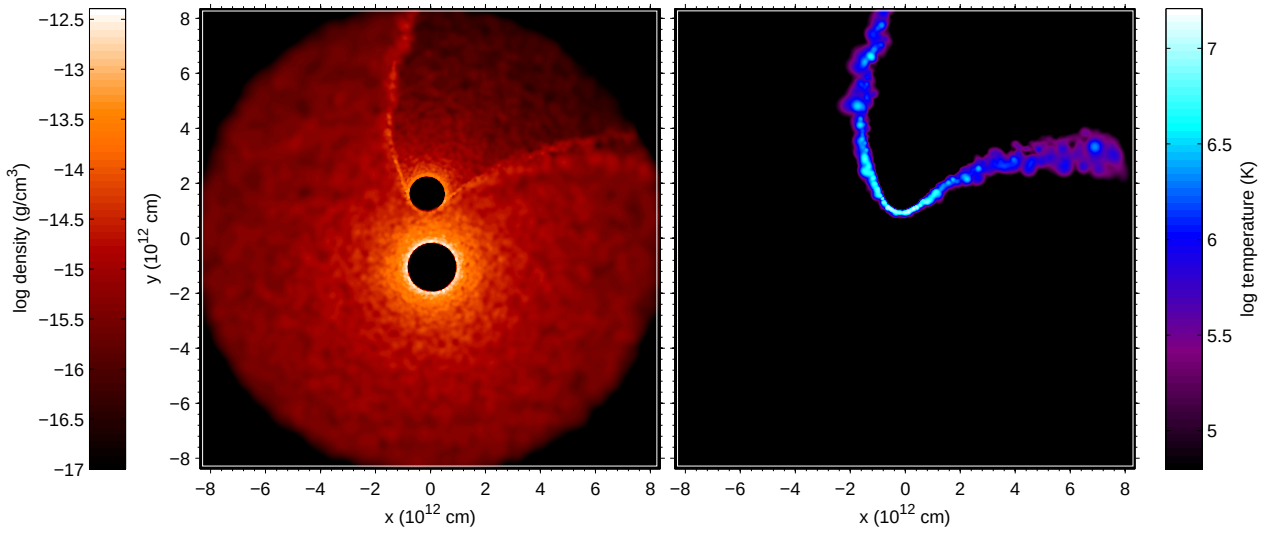

Figure 1. Hydrodynamic quantities in the orbital plane. The orbit is counterclockwise, the plot origin is the center of mass, and the simulation extends out to $r_{\max} = 3a$. The hot X-ray producing gas comes from the WSC and WWC.

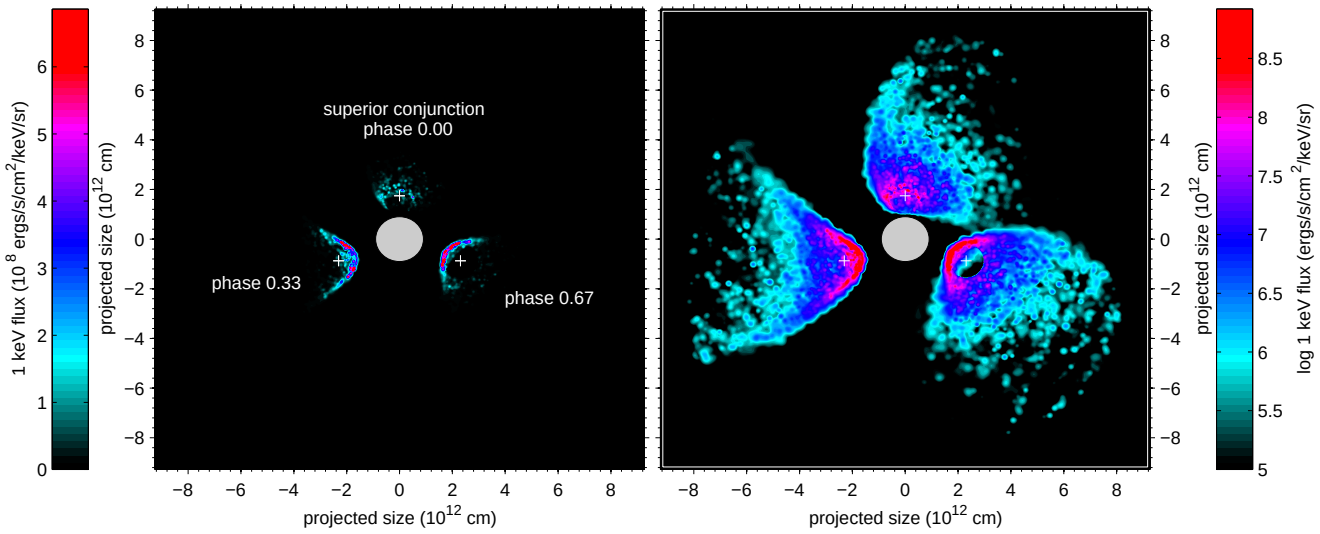

Figure 2. Surface brightness maps on a linear (left) and logarithmic scale (right) for the 1 keV band (specifically 0.9886–1.012 keV) shown in the reference frame of the O3 star (gray sphere). For each panel, the phases shown are 0.00 (superior conjunction, top), 0.33 (lower left), and 0.67 (lower right). The white '+' signs show the center of the O6 star for reference.

HD 150136 simulations at 3 phases from a single density and temperature output. The linear scale (left panel) shows where the dominant contribution to the X-ray flux is coming from at each phase, while the logarithmic scale (right panel) shows the full dynamic range of the X-ray emitting gas. The surface of the O6 star facing its companion and the off-center wind-wind collision region are clearly lit up, with most of the emission coming from the WSC. The O6 star is clearly outlined after inferior conjunction (phase 0.67, lower right portion of each panel) as it blocks the central region of X-ray emitting material. The pixel maps also show that the emission from the prograde region (phase 0.33, lower left portion) is stronger than the retrograde region (phase 0.67, lower right portion). This is expected (see e.g. Pittard 2009) since a larger fraction of the prograde wind collides more head-on than the retrograde wind, thus producing larger shock velocities and higher temperature gas. At superior conjunction (top portion), the inclination is too low to have the O3 star occult X-rays, but the extra absorption of X-rays causes a notable decline in surface brightness maps.

3 RESULTS: X-RAY LIGHT CURVE AND SPECTRA

In absolute units, Fig. 3 compares the zeroth-order, *Chandra* ACIS-S light curves of the model (red) and data (black). To decrease the fluctuations caused by the random injection of SPH particles, the model curve is averaged from 20 density and temperature outputs, and the grey shaded region shows the error at the 1-σ level of the resulting dispersion. The variation of the model light curve throughout the orbit in-

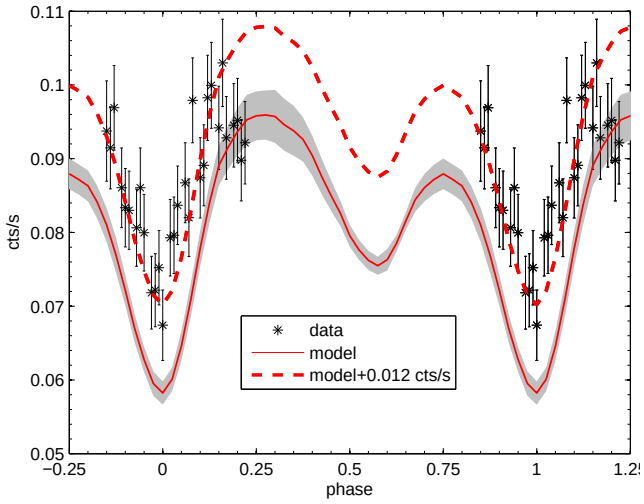

Figure 3. Model (red) and data (black) *Chandra* light curve. The shaded region (grey) shows the model 1-σ error. Adding 0.012 counts/s to the model (red dashed), which is presumably due to EWS emission, achieves good agreement over the limited phase coverage of the data.

dicates that the X-rays produced are always suffering from some degree of absorption by the O3 wind and/or occultation by the O6 star. The maximum of these two effects cause the dips in the light curve at superior conjunction (O3-wind absorption) and inferior conjunction (O6-star occultation). The asymmetry in flux before and after inferior conjunction arises from the difference in X-ray strength from the prograde to retrograde side of the wind; the weaker retrograde X-rays are occulted around phase 0.25, while the stronger prograde X-rays are occulted around phase 0.75, causing phase 0.25 to have the strongest X-ray emission over an orbital period.

The overall model flux is lower than the data, but this could be because the model does not account for embedded-wind-shock (EWS) emission from either star. The O3 star, specifically, should have appreciable EWS emission, and given that a large volume of the O3 wind is unperturbed by its companion or its companion's wind, a reasonable approximation is to add a constant flux to the WSC/WWC X-ray flux of the model to account for EWS emission. The dashed red curve shows the effect of adding 0.012 cts s^{-1}, which is plausible since the flux of HD 150135, a single O6V star in the same OB association, is ∼0.01 cts s^{-1} over the 0.5-5 keV band (S05).

The top panel of Fig. 4 compares the model (with no EWS contribution) and data for zeroth-order *Chandra* ACIS-S spectra (S05). The data spectrum (black) is extracted from the whole observation (phase 0.85-1.2), as is the model spectrum (red). Given that there are no parameters are adjusted to model the spectrum, the overall agreement is quite good. The model reproduces the three spectral lines identified by S05, with model line strengths approximately equal to that of the data. The soft 0.5–1.3 keV spectra match best, although the model slightly underpredicts the flux around 0.85 keV. Between the Mg XI line and Si XIII line the model produces too much flux, while above the Si XIII line the model produces too little flux.

The bottom of Fig. 4 shows the model spectral variation as a function of phase throughout the orbit. As expected, there are two clear trends showing how absorption (which affects the soft flux) and occultation (which equally affects all flux) determine the model spectral shape. A significant change in the soft spectra only occurs at superior conjunction (phase 0.0, blue), indicating the strong absorption by the O3 wind. On the other hand, the hard flux varies throughout the orbit; it is highest at superior conjunction, slightly lower, but approximately equal, at both quadratures (phase 0.25, red, and phase 0.75, black), and lowest at inferior conjunction (phase 0.5, green). This is because the hard X-ray flux is coming from the WSC around the O6 star, and the WSC is not occulted, partially occulted, and strongly occulted by the O6 star at superior conjunction, both quadratures, and inferior conjunction, respectively.

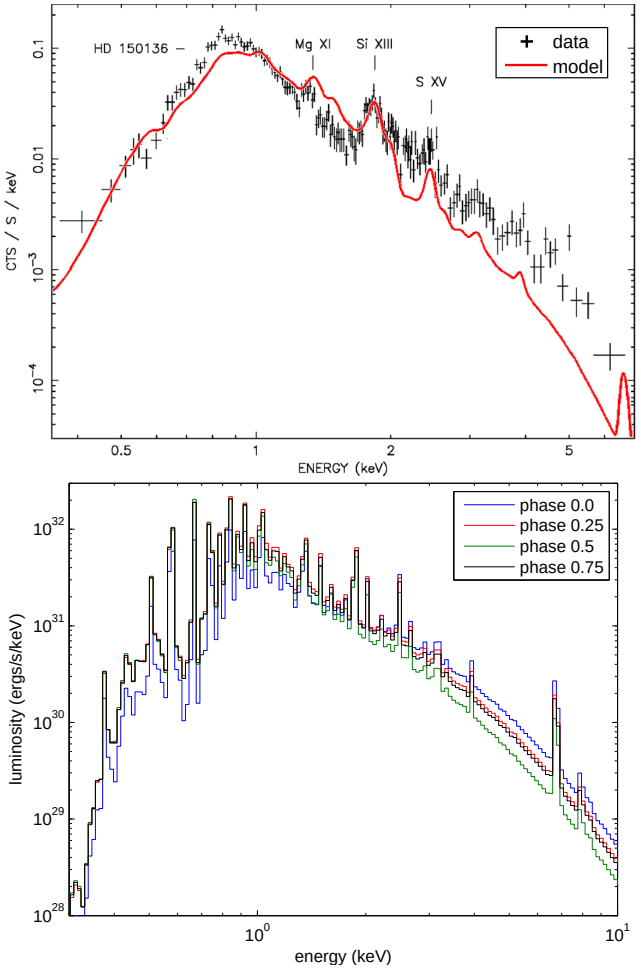

Figure 4. *Top*: Model zeroth-order *Chandra* ACIS-S spectra (red) overlaid on top of the data (black) from Fig. 7 of S05. *Bottom*: Predicted model luminosity as a function of phase.

4 DISCUSSION

The largest source of uncertainty in the model is the boundary implemented at the surface of the O6 star. The incoming O3 wind is subject to three radiative forces: its own radiation driving it towards the O6 star, the O6 wind driving it away from the O6 star, and the complicated issue of O3 radiation

reflecting off of the O6 stellar surface and driving the O3 wind away from the O6 star. Thus the density and temperature structure of the O3 wind in its deceleration/shock as it approaches the O6 star is subject to significant uncertainty, and generates uncertainty in the resulting X-ray observables. Earlier SPH models of HD 150136 (R13) did not have ghost particles, so the WSC shock was weaker, which led to much less X-ray production and variation: $\sim$0.025 cts s^{-1} at minimum to $\sim$0.04 cts s^{-1} at maximum. The ghost-particle implementation does a good job of inducing X-ray emission from the two expected regions, the WSC and WWC, and agrees quite well with the published observational data.

Over the limited phase coverage of the observation, the parameters of M12 did not need to be modified to fit the light curve trend around superior conjunction. However, the model of the X-ray observations provides a good test for the parameters of HD 150136. Nearly all parameters in Table 1, as well as β, affect the X-ray emission from the WSC, the WWC, or both, and the strong wind absorption at superior conjunction provides constraints on the O3 wind. In a follow-up paper (Leyder et al. 2014, *in prep.*), we will present new *Chandra* observations of HD covering an entire orbital period, at which time we will revisit both the O6-surface boundary condition and the parameters of HD 150136.

5 CONCLUSIONS AND FUTURE WORK

We model the *Chandra* X-ray observations of HD 150136 with 3D SPH and radiative transfer. The X-ray emission comes from two regions, the WSC, where the strong O3 wind reaches the O6 stellar star, and the WWC, which occurs off the line of centers. The model reproduces well the dip in the *Chandra* light curve around superior conjunction, and can match the absolute flux level if $\sim$0.012 cts s^{-1} of constant flux is assumed to come from the EWS X-rays from both stars. The model spectra also show many features of the *Chandra* spectrum, including the three prominent lines pointed out by S05, and good agreement in soft band. The hard model flux is below the observation, and if this permeates throughout the whole orbit, then it is difficult to invoke constant EWS emission to explain the difference in the model and observed light curves since their emission is generally soft. Combining this with other model uncertainties, particularly the difficult task of modeling the wind-star collision, we can only conclude qualitatively that the 3D SPH and radiative transfer model explain the *Chandra* data. The full orbit of data will help alleviate some of these challenges.

Looking to the future, we plan to implement several improvements to the SPH code, the most important two of which we mention here. Firstly, we will replace the random injection of wind particles with a more uniform injection. The random injection creates fluctuations in the SPH-kernel-averaged quantities (which is how hydrodynamic quantities are extracted from an SPH calculation), which can be seen in the variations in the density plot of Fig. 1, and leads to the model errors shown in Fig. 3. Initial tests of injecting particles from a uniform distribution on a sphere show that these variations are markedly decreased.

Secondly, since the kernel-averaged quantities are much smoother using a more uniform SPH particle injection, we will implement the CAK line force (Castor et al. 1975) for driving stellar winds into the code. This is more realistic than the anti-gravity-like radiative forces currently used, and thus will provide a more accurate model. The implementation of the line force also allows for the inclusion of radiative braking, which could be required if the full *Chandra* data set motivates changes in the parameters of HD 150136 in such a way that this phenomenon is now possible.

ACKNOWLEDGMENTS

CMPR acknowledges support from a NASA Delaware Space Grant Fellowship and a Japan Society for the Promotion of Science (JSPS) Obei-Tanki Fellowship. ATO acknowledges financial support from a JSPS grant (24540235). Resources supporting this work were provided by the NASA High-End Computing (HEC) Program through the NASA Advanced Supercomputing (NAS) Division at Ames Research Center.

REFERENCES

Arnaud K. A., 1996, in Jacoby G. H., Barnes J., eds, Astronomical Data Analysis Software and Systems V Vol. 101 of Astronomical Society of the Pacific Conference Series, XSPEC: The First Ten Years. p. 17
Bate M. R., Bonnell I. A., Price N. M., 1995, MNRAS, 277, 362
Benz W., Cameron A. G. W., Press W. H., Bowers R. L., 1990, ApJ, 348, 647
Castor J. I., Abbott D. C., Klein R. I., 1975, ApJ, 195, 157
Drew J. E., 1989, ApJS, 71, 267
Gayley K. G., Owocki S. P., Cranmer S. R., 1997, ApJ, 475, 786
Herbst W., Havlen R. J., 1977, A&AS, 30, 279
Leutenegger M. A., Cohen D. H., Zsargó J., Martell E. M., MacArthur J. P., Owocki S. P., Gagné M., Hillier D. J., 2010, ApJ, 719, 1767
Madura T. I., Gull T. R., Okazaki A. T., Russell C. M. P., Owocki S. P., Groh J. H., Corcoran M. F., Hamaguchi K., Teodoro M., 2013, ArXiv e-prints
Mahy L., Gosset E., Sana H., Damerdji Y., De Becker M., Rauw G., Nitschelm C., 2012, A&A, 540, A97
Monaghan J. J., 1992, ARA&A, 30, 543
Okazaki A. T., Owocki S. P., Russell C. M. P., Corcoran M. F., 2008, MNRAS, 388, L39
Owocki S. P., Cranmer S. R., Blondin J. M., 1994, Ap&SS, 221, 455
Pittard J. M., 2009, MNRAS, 396, 1743
Price D. J., 2007, PASA, 24, 159
Russell C. M. P., 2013, PhD thesis, University of Delaware
Skinner S. L., Zhekov S. A., Palla F., Barbosa C. L. D. R., 2005, MNRAS, 361, 191
Smith B., Sigurdsson S., Abel T., 2008, MNRAS, 385, 1443
Smith R. K., Brickhouse N. S., Liedahl D. A., Raymond J. C., 2001, ApJLett, 556, L91
Stevens I. R., Pollock A. M. T., 1994, MNRAS, 269, 226
Townsend R. H. D., 2009, ApJS, 181, 391
Wilms J., Allen A., McCray R., 2000, ApJ, 542, 914

This paper has been typeset from a TEX/ LATEX file prepared by the author.